Persistence of the large-scale interior deep ocean circulation
in global repeat hydrographic sections

Enter authors here: Susan L. Hautala[1] and Garrett Finucane[1†]

[1]School of Oceanography, University of Washington, Seattle.

Corresponding author: Susan Hautala (hautala@uw.edu)

†Currently at Department of Atmospheric and Oceanic Sciences, University of California Los Angeles.

Key Points:

- Large-scale density gradients in most parts of the deep ocean away from boundaries are stable over the modern observational period.
- The structure of large-scale (planetary) potential vorticity in the deep interior ocean is also persistent from occupation to occupation.
- These results support the assumption of quasi-steady state that underlies many analyses, including hydrographic inverse models.

Abstract

An assumption of steady-state is a common basis for deep ocean circulation theory and observational strategies. We use GO-SHIP's *Easy Ocean* uniformly gridded CTD data from repeat hydrographic sections to test this assumption. In particular, we ask: for what regions of the world ocean is there evidence that the planetary scale deep geostrophic shear and potential vorticity fields, related to potential density gradients, are in quasi steady-state over the past forty years? We find that away from boundary currents, planetary-scale potential density gradients in most parts of the deep ocean are stable from occupation to occupation, to within approximately 15% estimated standard error (lower in many parts of the global ocean interior), with higher variability in a few expected regions and for shorter sections.

Plain Language Summary

In analyzing ocean circulation, it is common practice to use all available density data, because doing so can average out short time scales of variability (hours to years) and provide values representative of an underlying circulation pattern that is persistent over time. In doing so, a "steady-state" assumption has been made – that the underlying ocean circulation does not have a long term trend over the four decades of the modern observational period. This assumption may be problematic given known warming of the deepest parts of the ocean. Our study uses data from a global collection of long sampling lines, repeated every decade or so, to test the steady-state assumption for the deep ocean's density field, and finds that it generally holds true, except near intense currents that occur at its lateral boundaries and in parts of the ocean close to the few locations where deep water is formed.

1 Introduction

An assumption of steady state is a fundamental tenet of both deep ocean circulation theory and observational strategies. This assumption has been widely applied, over time scales ranging from the multi-decadal span of the modern observational period (e.g., Talley et al. 2003; Lumpkin and Speer 2007; MacDonald et al. 2009; Khatiwala et al. 2012; Holzer et al. 2017) to millennial time scale (Gebbie and Huybers, 2019). By combining all available hydrographic data to estimate the large-scale geostrophic shear in a planetary geostrophic inverse calculation, the authors rely on steady-state in their recent deep circulation analyses for the Northeast Pacific Basin (Hautala, 2018; hereafter H18) and the Brazil Basin.

The physical basis, at least for a quasi-steady state, is often discussed in terms of the long adjustment time of the deep ocean, although faster teleconnection mechanisms have been proposed (Masuda et al. 2010). Stability of the large-scale circulation pattern during the modern observational period is supported by persistent conservative tracer features such as deep ^{3}He extrema (e.g., Lupton and Jenkins 2017; Takahata et al. 2018; Jenkins et al. 2020). On millenial timescales, Zhao et al. (2018) find consistency of the evolution of the deglacial deep radiocarbon field with atmospheric trends using modern ventilation rates, except in the northern North Atlantic and Southern Ocean, both close to the regions of active deep water formation.

On the other hand, given the recent observed changes in abyssal water mass temperature/salinity and also potentially in the rates of bottom water formation (e.g., Talley et al. 2015, and references therein; Voet et al. 2016; Volkov et al. 2016; Purkey et al. 2018; Purkey et al. 2019; Johnson et al. 2019; Johnson et al. 2020), it is important to revisit observational evidence that bears on the steady-state assumption. Here, we reframe the question into one that can be addressed by the existing observations along repeat hydrographic sections. We ask: for what regions of the world ocean is there evidence that the deep geostrophic shear (derived from large-scale gradients in potential density on isobaric surfaces) and planetary potential vorticity (derived from the vertical potential density gradient) are in a quasi steady-state over the past forty years? As a part of the answer to this question, we also estimate the standard error for planetary geostrophic scale variations of density and potential vorticity fields, based on a technique that smooths out the prominent mesoscale variability.

2 Data and Methods

We use the *GO-SHIP Easy Ocean* data product (Katsumata et al. 2021) that maps the GO-SHIP/CLIVAR/WOCE sections onto uniform space and pressure coordinates (Figure 1). The data for all sections was downloaded from their "clean" gridded CTD files. Conservative temperature and absolute salinity values, calculated using TEOS-10 (McDougall and Barker 2011) are already included in these files. Potential density is computed along each section at three pressures: P_1=2000, P_2=3000 and P_3=4000 dbar using the

gsw-python 0.1 (TEOS-10) codes *gsw.density.sigma2*, *gsw.density.sigma3* and *gsw.density.sigma4*. Large-scale potential vorticity (PV $= f/g\ N^2$) is calculated from N^2 using *gsw.stability*, and then vertically averaged over 200 m centered on each P_i.

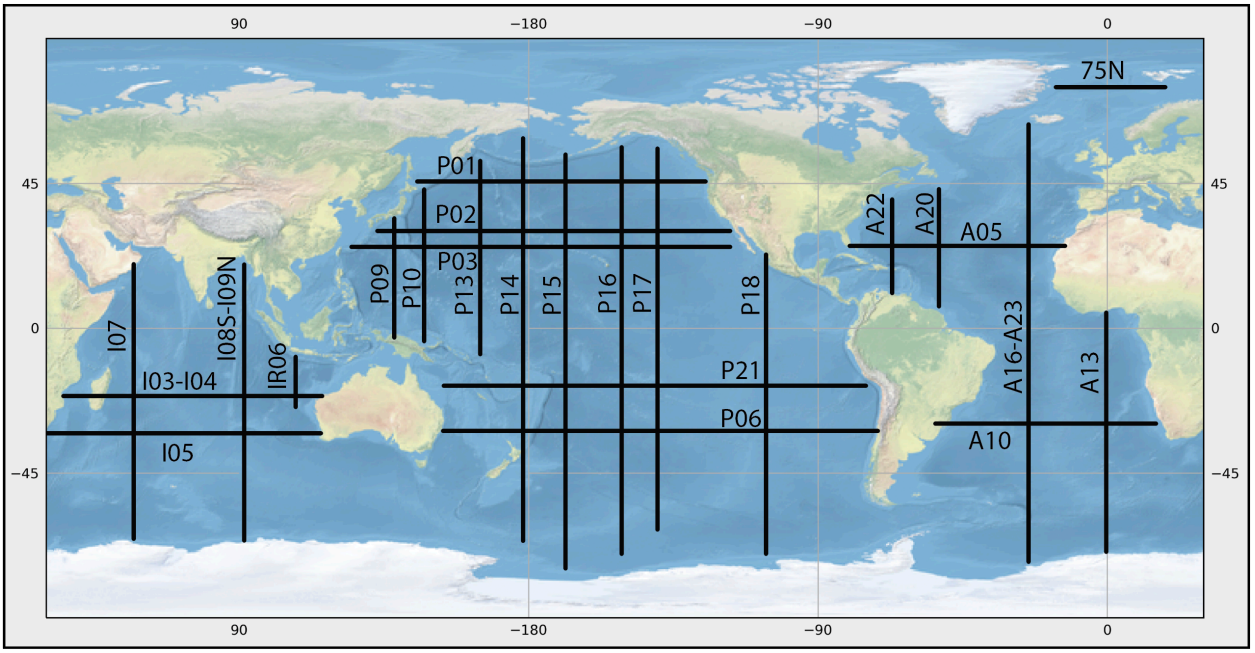

Figure 1. Nominal zonal and meridional locations of the *GO-SHIP Easy Ocean* compilation of uniformly gridded repeat hydrographic sections (Katsumata et al., 2021). Only sections (or parts of sections) with more than one occupation are included in this analysis.

Planetary-scale (i.e., order 1000 km horizontal length scale) spatial variations are assessed using fits produced by the *gamm* function from the *R* toolbox *mgcv*, with thin-plate spline (TPS) basis functions (Wood 2003). This is the univariate analog of the method (Trossman et al. 2011) that was used to determine the large-scale structure of deep ocean neutral density, potential vorticity and salinity fields in H18.

3 Results and Discussion

Potential density values at 2000, 3000, and 4000 dbar are shown in Figure 2 for representative sections. These sections were chosen for their greater length (allowing for more reliable detection of the large scale trend in the presence of eddy noise), with preference given to sections with more occupations. Because the 5000 dbar horizon is often split by topography into isolated deep basins, we do not analyze it for all sections, although $_4$ along this level is shown for selected sections in Figure 3. Several sections of potential vorticity are shown

in Figure 4. As contrasting examples, several shorter sections with forseeably larger noise to signal ratio are shown in in the online Supporting Information in Figure S1 (P09: running through the Philippine Sea; IR06: just downstream of the Indonesian Throughflow; and 75N: in the far subpolar North Atlantic). Remaining sections with more than one occupation are shown in Figures S2–S4.

Despite substantial mesoscale eddy noise, planetary-scale trends in the deep interior ocean (i.e., several hundred kilometers away from lateral boundaries) are remarkably similar from occupation to occupation (Figures 2 and 4, and online Supporting Information). Since the horizontal potential density gradient is related directly to the geostrophic shear through the thermal wind equation, these results imply that the interior abyssal circulation has not greatly changed over the modern observational period. Larger occupation-to-occupation variability occurs primarily in expected regions, particularly for shorter sections (Figure S1), in deep western boundary currents, and in wind-driven western boundary current extensions.

The Pacific Ocean has the largest number of repeat sections available and we discuss that basin first, and most extensively. As an example, consider the section at nominal 47°N in the subarctic Pacific (P01, Figure 2a), a key component of the inverse calculation of H18. This section has repeat data from 1985, 1999, 2007 and 2014. Along this section, potential density at 2000 dbar reaches a maximum at about 160°E and a broad minimum at about 160°W (Figure 2a, top panel). While this structure clearly persists from occupation to occupation, the extrema in the TPS fits (especially the western peak) shift slightly because of the configuration of eddies present in an individual section. We use this 40° longitude range for an example quantification of the slopes involved and their differences between occupations: the along-section potential density gradient at 2000 dbar in the TPS fit varies from -1.256×10^{-5} to -1.028×10^{-5} kg m^{-3} km^{-1}, with a mean value of -1.172×10^{-5} kg m^{-3} km^{-1}. From the thermal wind equation, this mean value is equivalent to a change of geostrophic velocity of 1 mm/s over 1000 m depth. The standard deviation of the four occupations is 6–7% of the average gradient for the 2000–4000 dbar range that we examined.

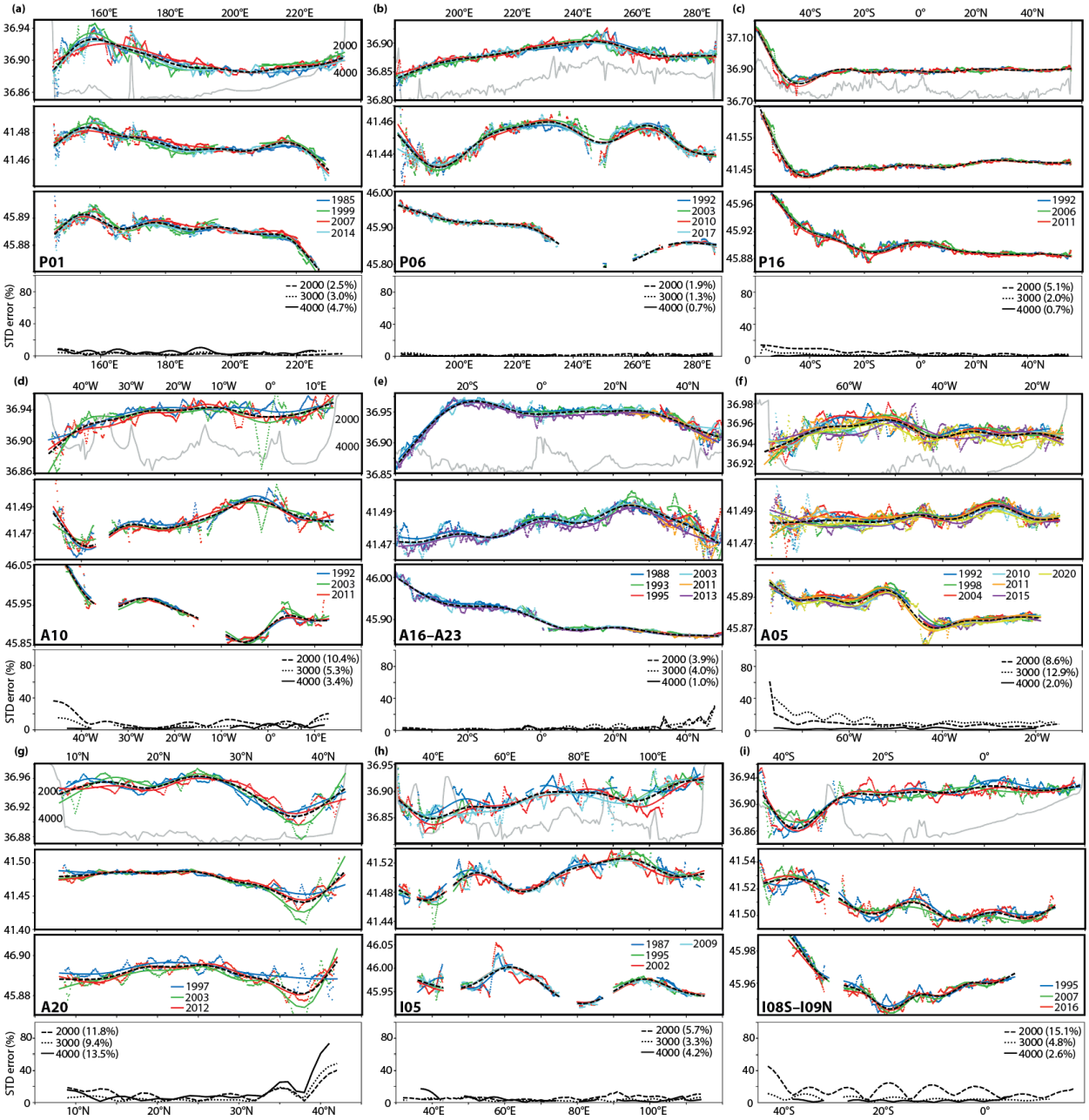

Figure 2. Representative sections from the Pacific (subplots a-c), Atlantic (d-g) and Indian Ocean (h, i). Dots in the top three-panels of each subplot show individual density values at 2000, 3000 and 4000 dbar levels ($_2$, $_3$ and $_4$ respectively, kg m^{-3}), colored by occupation year. Smooth colored lines show

two-dimensional thin-plate spline (TPS) fits to each occupation. The black dashed line shows the TPS fit using data from all years. In the top panel of each subplot, a gray curve shows the deepest point sampled, an indicator of bathymetry, according to the scale in the first column. The lower panel of each subplot shows percent standard error for density differences over 2° of the along-section coordinate (see text for details), with numbers in parentheses reporting the section average value.

Although helpful as an illustrative example, the previous calculation is dependent on its horizontal bounds, and so, in the lower panels of each subplot in Figure 2, we plot a relative error estimate along the entire section. The relevant quantity that varies between the uniformly gridded occupations is the local large-scale isobaric potential density difference ( ) between two points based on the smoothed TPS fits. We show the standard error of for 2° intervals along the section, where the number of degrees of freedom is the number of occupations. As the central tendency, we use the all-occupation TPS fit (shown in the upper three panels as a black dashed line), since the field produced by the large-scale mapping technique is the quantity of interest for quantification of error. While the technique returns its own estimates of mapping error that are used in the inverse analyses, those values are still dependent on the assumption that the underlying field of interest is not changing between occupations.

Since the range of potential density varies considerably with depth and between basins, we have normalized values using the interquartile range of potential density at each level and section, taken from the all-occupation TPS fit. Because of this normalization choice, the error estimates are not true percentages of at their corresponding point in space along the section. However, this choice avoids the tendency for the ratio to blow up as the local approaches zero. It is apparent that for many longer sections, deep interior ocean density differences over large scales can be estimated with a relatively low margin of error. For example, for P01, the mean standard error for all three pressure levels ranges from 2 to 5% of the normalization values at those depths. 95% confidence error bars would be about two to three times larger, given the low number of degrees of freedom.

Moving deeper within P01 (Figure 2a), at the the 3000 and 4000 dbar levels we find another prominent and persistent structure in the form of a marked decrease in density on level surfaces approaching the eastern end of the section, noted in the very first occupation by Talley et al. (1991). This feature is the thermal wind signature of a broad bottom-intensified southward flow that carries Upper Circumpolar Deep Water away from its sources in the Aleutian Trench to supply much of the Northeast Pacific Basin north of 30°N (H18). The structure in potential vorticity at 4000 dbar in this region also is stable over time (Figure 4b). PV decreases approaching the eastern edge along neutral surfaces (H18), and the increase observed here on level surfaces is convolved with the strong downward slope of neutral surfaces as they ground into rising topography on their eastern edges. This zonal structure in PV is important because it supports

meridional flow in the presence of weak diapycnal mixing (H18).

In the first reoccupation of P01 in 1999, a warming of about 0.005°C below 5000 m was observed (Fukasawa et al. 2004). Given values of $\quad = 1.2$°C and $S = 34.68$ psu from the WOCE Atlas (Talley 2007), that degree of temperature change would correspond to a decrease in $_4$ of 0.0008 kg m^{-3}, a small number relative to the planetary-scale horizontal variation at 5000 dbar (Figure 3a). The most recent occupation of this section does show a distinct reduction in density in selected areas, particularly around the dateline, but density differences across the entire basin remain robust and the section-average standard error in the large-scale trend at 5000 dbar is only 1% of the normalization value (Figure 3a).

P06, along nominal 30°S, demonstrates the persistence of deep zonal potential density gradients (hence geostrophic shear of the meridional flow) in the South Pacific subtropical interior (Figure 2b). As just discussed for the subarctic section, this result is not inconsistent with the observations of Sloyan et al. (2013) of bottom water warming and even a weakening of the northward AABW transport – the focus of those changes is around neutral density 28.2 kg m^{-3}, lying deeper, at about 5000 dbar, and, as they note, those changes are largely confined to the western boundary region. Even though the reduction in density between 1992 and 2017 is clear west of 155°W/205°E (Figure 3b), its relatively small magnitude only impacts the shear in this area of relatively weak horizontal density gradient; the stronger shear zone located to the east of 155°W is robust, and the section-average standard error for the large-scale fit is only 0.3%.

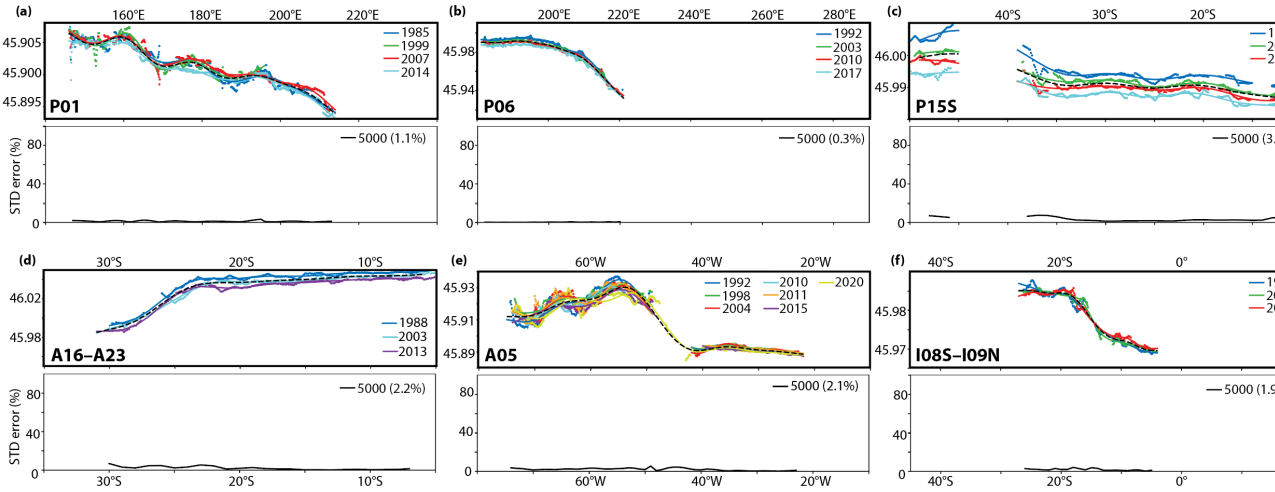

Figure 3. As in Figure 2, but for potential density ($_4$) along the 5000 dbar horizon, for selected sections.

Thus, both the subarctic (Figure 2a) and subtropical (Figure 2b, S2a-c) zonal density gradients in the Pacific Ocean are persistent over the modern observa-

tional period (note that some of the more variable longitude bands in Figure S2a can be attributed to an incomplete section in 1993 that distorts the TPS fit to that occupation of P02). Long meridional sections also demonstrate persistence of structure in density gradients, as exemplified for the Pacific by P16 (Figure 2c; see Figs S1d-i for other Pacific meridional sections). Even in the southernmost part of P16, extending into the stronger density gradients associated with the deep Antarctic Circumpolar Current, persistence over its twenty year observational span is observed. (While Southern Ocean persistence is observed for the other meridional sections, the southernmost latitudes of those sections have been truncated in the supplemental figures to enhance the subtropical variations and make the error estimates more relevant to those latitudes.) Greater variation among occupations tends to occur mostly in the western part of the North Pacific, especially in the vicinity of the deep Kuroshio Extension and in the Philippine Sea (Figures S1a, S2a,b,d,e). However, even along the 5000 dbar horizon in the deepest part of the western South Pacific, where the density reduction associated with global warming is most apparent, the planetary-scale density gradient structure is remarkably consistent, and can be estimated with a mean standard error of 3.3% (Figure 3c).

Given the large extent of the Pacific Ocean, one could argue it is the most likely to show persistence both because the planetary scale fit can average out many mesoscale features, and because its interior is relatively isolated from modern changes communicated via deep western boundary currents. However, persistence is also observed in typically shorter sections in the interior Atlantic and Indian Ocean sections (Figures 2d-f, S3, S4).

For example, for the A10 section across nominal 30°S in the South Atlantic (Figure 2d), the normalized error is greatest at 2000, but note that the mean zonal density gradients at mid-depth are weak. For the interior, the standard error still only reaches ~20% of its normalization value in certain longitude ranges where the configuration of eddies leads to subtle shifts in the smoothed curves, and the section average error is about half of that. Although the 4000 dbar horizon is broken up into segments by topography, there is clear persistence, in either raw or TPS curves, of the zonal density gradient. For the longitude range 15°-30°W, persistence is particularly important because it is related to the meridional geostrophic shear just north of the Hunter Channel. As in the western South Pacific, persistence does not contradict significant warming observed below 4000 m for Brazil Basin (Johnson et al. 2020). The density gradient along A16-A23 in this latitude range is surprisingly stable, despite the reduction in overall density (Figure 3d).

In the North Atlantic, variation from occupation to occupation tends to be somewhat larger, particularly for several quite short sections in its western and subpolar areas (Figures 2g, S1c, S3b), but estimated errors are still fairly low away from the deep Gulf Stream extension and far northern subpolar gyre, and there is a tendency for even lower variability at 4000 m than at mid-depth. A good example for this basin is A05 across the mid-latitude North Atlantic

(Figure 2f). That the western mid-depth North Atlantic has variable meridional geostrophic shear over large scales was first noted by Wunsch and Roemmich (1985; see their Figure 1a comparing 1981 and 1957 occupations along ~24°N). The likely cause is the well-known property and layer thickness anomalies over broad scales that have been attributed to interannual variability in the Upper North Atlantic Deep Water components (e.g., Curry et al. 1998; Ortega et al. 2017). Changes in the mean density of the far northern subpolar Atlantic section (Figure S1c) are striking and it is perhaps surprising that the basin-scale density gradients from year to year are even somewhat reproducible (except near the western boundary). This section, close to the sources of North Atlantic Deep Water would obviously be need to be treated with great caution in any steady-state inverse calculation.

Indian Ocean sections (Figures 2h,i and S4), although few in number, provide further support for the general conclusion of persistence, except near boundaries. More variability is observed, not surprisingly, in a short section across the Indonesian Throughflow as it enters the eastern Indian Ocean (IR06, Figure S1b). Although the Indian Ocean mean normalized errors are higher than the other basins (Table S1), two of the five sections have only been occupied twice (Figure S4), reducing the number of degrees of freedom. Additionally, with so few lines, a highly variable section such as IR06 is likely over-weighted in the average. Importantly, deep planetary scale density gradients along I05 are quite persistent (Figure 2h). The stability of this section, along with the other two zonal sections along ~30°S (Figure 2b, d), is important because they capture the global deep connection between the deep basins and the Southern Ocean.

In some regions mesoscale features repeat in the same location from occupation to occupation and are likely part of the slowly varying general circulation rather than transient eddies. These features are often associated with topography. For example, along I05 (Figure 2h), the sign of the shear in meridional velocity at 4000 dbar changes sign in each of the three sections at the same location (55°E–60°E) above the eastern flank of the Southwest Indian Ridge where the section crosses meridionally-oriented fracture zone canyons. Another example is meridional velocity shear of alternating sign along P01 within the deepest part of the Northwest Pacific Basin, just west of the Emperor Seamount Chain at ~170°E (Figure 2a). Along P16 in the South Pacific, the sign of the shear in zonal velocity along 4000 dbar changes signs multiple times between 15°S to 50°S, in nearly identical locations in each of its three occupations. The region between 30–50°S where the largest such alternations occur is within a deep basin bounded by slopes associated with the Pacific-Antarctic Ridge and Austral Islands (French Polynesia). Numerous examples from other sections can also be discerned (see online Supporting Information).

Potential vorticity (PV) in meridional sections largely tracks planetary vorticity in the deep ocean. However, the repeat hydrographic sections reveal deviations from this trend, over both large and regional scales, that are also stable from occupation to occupation. This is perhaps not surprising given the general

persistence of the density field itself, but is worthwhile examining separately since PV conservation underpins the inverse method of H18, as well as a whole class of earlier techniques going back to the beta spiral (Schott and Stommel 1978). Warming of the bottom water has also been associated with a reduction in stratification, and hence could impact planetary potential vorticity trends along the sections. However, as with the warming signal itself, substantial systematic changes are found deeper than about 5000 m (Zhang et al. 2021).

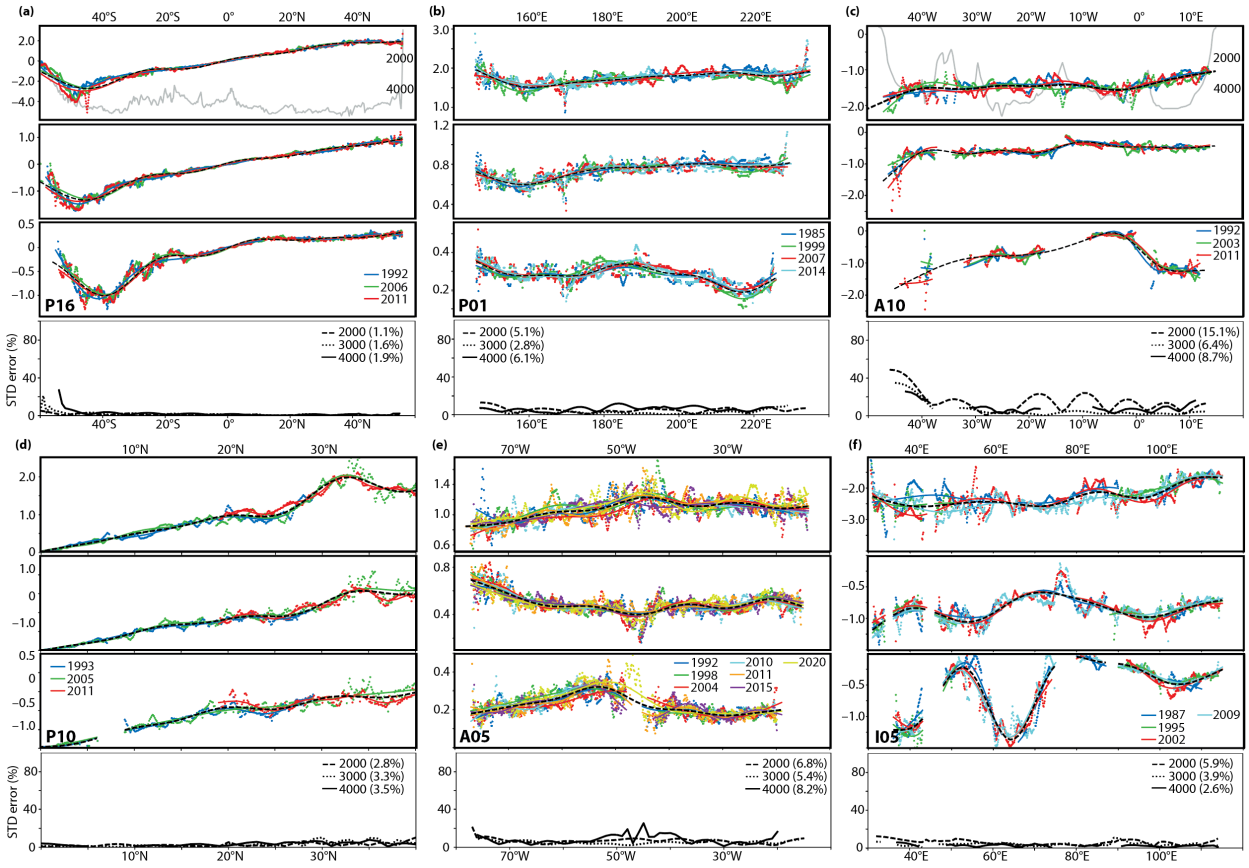

Figure 4. As in Figure 2, but for planetary potential vorticity in units of 10^{-11} m^{-1} s^{-1} for selected sections.

A marked reduction of the meridional PV gradient at the 4000 dbar level in the North Pacific (Figure 4a) is likely related to enhanced bottom mixing (Roussenov et al. 2002), perhaps enhanced by broad geothermal heating (Warren et al. 1986). In the South Pacific, PV goes through a notable minimum just equatorward of the Antarctic Circumpolar Current (Figure 4a, also other sections, not shown). In the southernmost part of P16, the absolute value of PV increases moving northwards towards its negative minimum. This trend is a consequence of increasing stratification along pressure surfaces that cross the

strongly downward tilting isopycnals, associated geostrophically with the relatively strong deep ACC. As previously discussed, a similar effect can be seen in the zonal increase in PV at 4000 dbar along P01 near their eastern edge where isopycnals dive into topography (Figure 4b). This convolution highlights that PV on neutral surfaces, rather than isobars, is the more useful quantity for oceanographic interpretation and inverse modeling. Although neutral surface PV is not specifically analyzed here, we hypothesize that its planetary-scale variations also likely to be persistent over the modern observational period since both isobaric density and PV gradients are stable.

As with the geostrophic shear, mesoscale PV variations that are likely part of the time-mean circulation can also be discerned. One example can be found in P10 in the western Pacific (Figure 4d) at about 25°N, where the PV gradient is weaker than expected from the planetary trend. In two of the three occupations, the PV gradient even reverses sign at 4000 dbar between 20-25°N. This is a region, complicated by zonally-oriented seamount chains, where Wijffels et al. (1998) identified an eastward current with a benthic water mass front at 25°N from 4000 m to the bottom. Potential density persistently decreases to the north (Figure 4d), associated with this bottom-intensified eastward flow. Wijffels et al. (1998) proposed that the eastward flowing water is sourced from lower latitude in a narrow boundary current steered west of the section by topography, likely influencing the regional PV gradient (see their Figure 10). Other illustrative examples are lower PV on either flank of the Mid-Atlantic Ridge in A05 (Figure 4e) and the topographically co-located variations on both planetary and mesoscales along I05 (Figure 4f).

5 Conclusions

The main conclusion of this study is that, while a considerable amount of mesoscale eddy variability can be seen between occupations, the underlying planetary scale pattern of isobaric density and potential vorticity in most of the deep global interior is unchanging. Furthermore, density gradients can currently be estimated, using an appropriate technique for capturing the largest scales of variation, to within approximately 15% estimated standard error (Table S1), with higher variability in a few expected regions and for shorter sections. As the number of occupations increases, the error level will drop further. Gradients for many areas of the deep interior, especially at 3000 and 4000 dbar, can be estimated with even lower error levels (<10%). Because of the relationship between density gradients and planetary geostrophic shear and dynamics, we infer that the deep ocean circulation is in a quasi-steady state over the modern observational period.

These results are not inconsistent with observed warming, in many parts of the global ocean, of the densest water below about 4000 m depth (e.g., Purkey et al., 2018, and references therein). However, the deep geostrophic shear is relatively unaffected, except in regions of weak shear, or adjacent to deep western boundary currents or otherwise directly influenced by changes in deep water formation. Thus, analyses can consistently combine all available data to make

progress toward a first order understanding of the interior deep ocean circulation, a picture that is currently fuzzy, at best. While it is entirely possible that over time the geostrophic shear in the deepest basins may begin to change, this eventuality may not present an immediate limitation for such analyses. For example, the planetary geostrophic inverse technique of H18 relies only on a thick layer of deep and mid-depth surfaces that are dynamically connected over basin scales, whereas the greatest warming signature occurs in the bottom water of deep basins that are often disconnected from one another by intervening topography. Given the support demonstrated here for the underlying assumption of quasi-steady state for depths between 2000 to 4000 dbar, this technique, along with many others developed in recent years, have the potential to yield first-order estimates of the deep circulation for much of the global ocean.

Acknowledgments and Data

The *GO-SHIP Easy Ocean data* (doi: 10.7942/GOSHIP-EasyOcean) are available at https://cchdo.ucsd.edu/products/goship-easyocean. The gsw-python codes are available at https://teos-10.github.io/GSW-Python/index.html. SH was partially supported by sabbatical leave from the University of Washington.

References

Curry, R. G., McCartney, M. S., & Joyce, T. M. (1998). Oceanic transport of subpolar climate signals to mid-depth subtropical waters. *Nature*, *391*(6667), 575–577. https://doi.org/10.1038/35356

Fukasawa, M., Freeland, H., Perkin, R., & Watanabe, T. (2004). Bottom water warming in the North Pacific Ocean. *Nature*, *427*(6977), 825–827. https://doi.org/10.1038/nature02337

Gebbie, G., & Huybers, P. (2018). The Little Ice Age and 20th-century deep Pacific cooling. *Science*, *363*(6422), 70–74. https://doi.org/10.1126/science.aar8413

Hautala, S. L. (2018). The abyssal and deep circulation of the Northeast Pacific Basin. *Progress in Oceanography*, *160*, 68–82. https://doi.org/10.1016/j.pocean.2017.11.011

Holzer, M., DeVries, T., Bianchi, D., Newton, R., Schlosser, P., & Winckler, G. (2017). Objective estimates of mantle 3He in the ocean and implications for constraining the deep ocean circulation. *Earth and Planetary Science Letters*, *458*, 305–314. https://doi.org/10.1016/j.epsl.2016.10.054

Jenkins, W. J., Hatta, M., Fitzsimmons, J. N., Schlitzer, R., Lanning, N. T., Shiller, A., et al. (2020). An intermediate-depth source of hydrothermal 3He and dissolved iron in the North Pacific. *Earth and Planetary Science Letters*, *539*, 116223. https://doi.org/10.1016/j.epsl.2020.116223

Johnson, G. C., Purkey, S. G., Zilberman, N. V., & Roemmich, D. (2019). Deep Argo Quantifies Bottom Water Warming Rates in the Southwest Pacific Basin. *Geophysical Research Letters*, *46*(5), 2662–2669. https://doi.org/10.1029/2018gl081685

Johnson, G. C., Cadot, C., Lyman, J. M., McTaggart, K. E., & Steffen, E. L. (2020). Antarctic Bottom Water Warming in the Brazil Basin: 1990s Through 2020, From WOCE to Deep Argo. *Geophysical Research Letters*, *47*(18). https://doi.org/10.1029/2020gl089191

Katsumata, K., Purkey, S., Cowley, R., Sloyan, B., Stephen, D., Moore, T., Talley, L., and Swift, J. (2021). GO-SHIP Easy Ocean: Formatted and gridded ship-based hydrographic section data, EGU General Assembly 2021, online, 19–30 Apr 2021, EGU21-3619, https://doi.org/10.5194/egusphere-egu21-3619, 2021.

Khatiwala, S., Primeau, F., & Holzer, M. (2012). Ventilation of the deep ocean constrained with tracer observations and implications for radiocarbon estimates of ideal mean age. *Earth and Planetary Science Letters*, *325*, 116–125. https://doi.org/10.1016/j.epsl.2012.01.038

Lumpkin, R., & Speer, K. (2007). Global Ocean Meridional Overturning. *Journal of Physical Oceanography*, *37*(10), 2550–2562. https://doi.org/10.1175/jpo3130.1

Lupton, J. E., & Jenkins, W. J. (2017). Evolution of the south Pacific helium plume over the past three decades. *Geochemistry, Geophysics, Geosystems*, *18*(5), 1810–1823. https://doi.org/10.1002/2017gc006848

Macdonald, A. M., Mecking, S., Robbins, P. E., Toole, J. M., Johnson, G. C., Talley, L., et al. (2009). The WOCE-era 3-D Pacific Ocean circulation and heat budget. *Progress in Oceanography*, *82*(4), 281–325. https://doi.org/10.1016/j.pocean.2009.08.002

McDougall, T.J. and P.M. Barker (2011). *Getting Started with TEOS-10 and the Gibbs Seawater (GSW) Oceanographic Toolbox*, SCOR/IAPSO WG127, ISBN 978-0-646-55621-5, 28pp.

Masuda, Awaji, T., Sugiura, N., Matthews, J. P., Toyoda, T., Kawai, Y., et al. (n.d.). Simulated Rapid Warming of Abyssal North Pacific Waters. *Science*, *329*, 319–329. https://doi.org/10.1126/science.1188703

Ortega, P., Robson, J., Sutton, R. T., & Andrews, M. B. (2017). Mechanisms of decadal variability in the Labrador Sea and the wider North Atlantic in a high-resolution climate model. *Climate Dynamics*, *49*(7–8), 2625–2647. https://doi.org/10.1007/s00382-016-3467-y

Purkey, S. G., Jr., W. M. S., Gebbie, G., Gordon, A. L., Sonnerup, R. E., Warner, M. J., & Bullister, J. L. (2018). A Synoptic View of the Ventilation and Circulation of Antarctic Bottom Water from Chlorofluorocarbons and Natural Tracers. *Annual Review of Marine Science*, *10*(1), 503–527. https://doi.org/10.1146/annurev-marine-121916-063414

Purkey, S. G., Johnson, G. C., Talley, L. D., Sloyan, B. M., Wijffels, S. E., Smethie, W., et al. (2019). Unabated Bottom Water Warming and Freshening in the South Pacific Ocean. *Journal of Geophysical Research: Oceans …*, *124*(3), 1778–1794. https://doi.org/10.1029/2018jc014775

Roussenov, V., Williams, R. G., & O'Dwyer, J. (2002). Formation of Low Potential Vorticity over the Deep Pacific. *Journal of Physical Oceanography*, *32*(6), 1811–1823. https://doi.org/10.1175/1520-0485(2002)032%3c1811:folpvo%3e2.0.co;2

Schott, F., & Stommel, H. (1978). Beta spirals and absolute velocities in different oceans. *Deep Sea Research*, *25*(11), 961–1010. https://doi.org/10.1016/0146-6291(78)90583-0

Sloyan, B. M., Wijffels, S. E., Tilbrook, B., Katsumata, K., Murata, A., & MacDonald, A. M. (2013). Deep ocean changes near the western boundary of the South Pacific Ocean. *Journal of Physical Oceanography*, *43*(10), 2132–2141. https://doi.org/10.1175/jpo-d-12-0182.1

Schott, F., & Stommel, H. (1978). Beta spirals and absolute velocities in different oceans. *Deep Sea Research*, *25*(11), 961–1010. https://doi.org/10.1016/0146-6291(78)90583-0

Talley, L.D. (2007). Hydrographic Atlas of the World Ocean Circulation Experiment(WOCE). Volume 2: Pacific Ocean. International WOCE Project Office, Southampton,U.K.

Talley, L. D., T. M. Joyce and R. A. de Szoeke (1991), Transpacific sections at 47°N and 152°W: distribution of properties. *Deep-Sea Research*, 38 (S1): S63-S82.

Talley, L. D., Reid, J. L., & Robbins, P. E. (2003). Data-Based Meridional Overturning Streamfunctions for the Global Ocean. *Journal of Climate*, *16*(19), 3213–3226. https://doi.org/10.1175/1520-0442(2003)016<3213:dmosft>2.0.co;2

Talley, L. D., Feely, R. A., Sloyan, B. M., Wanninkhof, R., Baringer, M. O., Bullister, J. L., et al. (2015). Changes in Ocean Heat, Carbon Content, and Ventilation: A Review of the First Decade of GO-SHIP Global Repeat Hydrography. *Annual Review of Marine Science*, *8*(1), 1–31. https://doi.org/10.1146/annurev-marine-052915-100829

Trossman, D. S., Thompson, L. A., & Hautala, S. L. (2011). Application of thin-plate splines in two dimensions to oceanographic tracer data. *Journal of Atmospheric …*, *28*, 1522–1538. https://doi.org/10.1175/jtech-d-10-05024.1

Voet, G., Alford, M. H., Girton, J. B., Carter, G. S., Mickett, J. B., & Klymak, J. M. (2016). Warming and Weakening of the Abyssal Flow through Samoan Passage. *Journal of Physical Oceanography*, *46*(8), 2389–2401. https://doi.org/10.1175/jpo-d-16-0063.1

Volkov, D. L., Lee, S., Landerer, F. W., & Lumpkin, R. (2017). Decade-long deep-ocean warming detected in the subtropical South Pacific. *Geophysical Research Letters*, *44*(2), 927–936. https://doi.org/10.1002/2016gl071661

Warren, B. A., Talley, L. D., & Joyce, T. M. (1986). The geothermal heating of the abyssal subarctic Pacific Ocean. *Deep Sea Research Part A …*, *33*(8),

1003–1015. https://doi.org/10.1016/0198-0149(86)90026-9

Wijffels. S. E., M. M. Hall, T. Joyce, D. J. Torres, P. Hacker and E. Firing (1998). Multiple deep gyres of the western North Pacific: A WOCE section along 149°E. J. Geophys. Res. 103 (C6): 12,985-13,009.

Wunsch, C., & Roemmich, D. H. (1985). Is the North Atlantic in Sverdrup Balance? *Journal of Physical Oceanography*, *15*, 1876–1880.

Wood, S. N. (2003). Thin plate regression splines. *Journal of the Royal Statisitcal Society, Series B*, *65*, 95–114.

Zhang, H. J., Whalen, C. B., Kumar, N., & Purkey, S. G. (2021). Decreased stratification in the abyssal southwest Pacific basin and implications for the energy budget. *Geophysical Research Letters*, *48*(19). https://doi.org/10.1029/2021gl094322

Zhao, N., Marchal, O., Keigwin, L., Amrhein, D., & Gebbie, G. (2018). A Synthesis of Deglacial Deep-Sea Radiocarbon Records and Their (In)Consistency With Modern Ocean Ventilation. *Paleoceanography and Paleoclimatology*, *33*(2), 128–151. https://doi.org/10.1002/2017pa003174